Article

Not peer-reviewed version

Exploring the Binding Landscape of a Small Set of Natural Products Targeting the KRAS22-RT G-Quadruplex

Maria Marzano , Maria Grazia Nolli , Claudia Pagano , Monica Scognamiglio , Giovanna Valentino , Brigida D'Abrosca , Paola Poma , Monica Notarbartolo , Serena Riela * , Antonio Fiorentino * , Stefano D'Errico * , Nicola Borbone *

Posted Date: 20 April 2026

doi: 10.20944/preprints202604.1302.v1

Keywords: G-quadruplex; KRAS gene; KRAS22-RT oligonucleotide; Mediterranean plants; natural products; alkaloids; CD spectroscopy; NMR

 doi:10.20944/preprints202604.1302.v1

Article

Exploring the Binding Landscape of a Small Set of Natural Products Targeting the KRAS22-RT G-Quadruplex

Maria Marzano [1,†], Maria Grazia Nolli [2,†], Claudia Pagano [2], Monica Scognamiglio [3], Giovanna Valentino [3], Brigida D'Abrosca [3], Paola Poma, [4] Monica Notarbartolo [4], Serena Riela [5,*], Antonio Fiorentino [3,*], Stefano D'Errico [2,*] and Nicola Borbone [2,*]

[1] Centro di Servizio di Ateneo per le Scienze e Tecnologie per la Vita (CESTEV), University of Napoli Federico II, via Tommaso De Amicis 95, 80145 Napoli, Italy

[2] Department of Pharmacy, University of Napoli Federico II, via Domenico Montesano 49, 80131 Napoli, Italy

[3] Department of Environmental Biological and Pharmaceutical Sciences and Technologies, University of Campania Luigi Vanvitelli, Via Vivaldi 43, 81100 Caserta, Italy

[4] Department of Biological, Chemical and Pharmaceutical Science and Technology, University of Palermo, Palermo, 90128, Italy

[5] Department of Chemical Sciences, University of Catania, Viale Andrea Doria 6, Catania, 95125, Italy

* Correspondence: serena.riela@unict.it (S.R.); antonio.fiorentino@unicampania.it (A.F.); stefano.derrico@unina.it (S.D.); nicola.borbone@unina.it (N.B.)

† These authors contributed equally.

Abstract

Herein, we investigated the binding properties of four natural compounds extracted from Mediterranean plants—distachyasin, CxB, CxC, and magnoflorine—toward the G-quadruplex (GQ) formed by the KRAS22-RT sequence, a modified KRAS-derived oligonucleotide commonly used as a model of the KRAS oncogene, which adopts a single, well-defined parallel intramolecular GQ structure. Circular dichroism (CD) and nuclear magnetic resonance (NMR) spectroscopies revealed that distachyasin, CxC, and magnoflorine induced only a slight stabilization of the GQ. In contrast, CxB significantly increased the GQ melting temperature, indicating a markedly stronger stabilizing effect. Notably, the reduced stabilizing effect of its diastereomer CxC highlights how the spatial arrangement of substituents around the core structure can strongly influence the binding properties of ligands towards GQs. Finally, the compounds were evaluated in three breast cancer cell lines and showed antiproliferative effects, particularly in the drug-resistant model.

Keywords: G-quadruplex; KRAS gene; KRAS22-RT oligonucleotide; Mediterranean plants; natural products; alkaloids; CD spectroscopy; NMR

1. Introduction

Mediterranean plants constitute a valuable reservoir of bioactive secondary metabolites characterized by remarkable structural diversity and by the ability to interact with a broad range of biological targets. [1–3] These compounds often display potent pharmacological activities across diverse therapeutic areas, including aging, [4,5] oncology, infectious diseases, and neurodegeneration. [6–8] Owing to their therapeutic potential, they have long been explored either as direct pharmacological agents or as structural scaffolds for the development of novel drugs targeting various diseases. In recent years, increasing attention has been directed toward their potential to target non-canonical nucleic acid structures, particularly G-quadruplexes (GQs). [9,10] GQs are DNA secondary structures formed by guanine-rich sequences, that assemble into stacked G-tetrads stabilized by Hoogsteen hydrogen bonds. [11] Found both in DNA and RNA, GQs exhibit

 doi:10.20944/preprints202604.1302.v1

considerable topological diversity, adopting parallel, antiparallel, or hybrid conformations, depending on the DNA sequence and ionic conditions. [12] The evidence of GQs formation in vivo [13] has strengthened their relevance as therapeutic targets, especially in cancer and neurodegenerative diseases. [14–16] In fact, the therapeutic outcome of GQ targeting is context-dependent: in oncology, stabilizing GQs using exogenous ligands, particularly at telomeric and promoter regions of human genome, [17] can impair cancer cell proliferation by interfering with telomerase activity and oncogene expression; conversely, in neurodegenerative diseases, where the abnormal amplification of GQ-forming repeats results in pathological DNA aggregation and impaired gene regulation, destabilization of GQ structures by interaction with ligands may offer a promising strategy to restore the normal cellular function. [18] The structural complexity of natural products makes them particularly well-suited to interact with the dynamic and polymorphic nature of GQs, [19–22] showing, in some cases, a high degree of binding selectivity with respect to the duplex DNA. [9,23–25]

KRAS oncogene is widely recognized as one of the most frequently overexpressed oncogenes in human malignancies. [26,27] It is strongly associated with poor patient outcomes, particularly in pancreatic, colorectal, and lung cancers. Although KRAS mutations are exceptionally rare in breast cancer, they are more frequently implicated through deregulation of downstream signaling such as PI3K/AKT and MAPK pathways, affecting over 20% of tumors. [28,29] In basal-type (triple-negative) breast cancer models, KRAS is preferentially activated and plays a pivotal role in maintaining mesenchymal features and promoting metastatic behavior via SLUG-mediated epithelial–mesenchymal transition. [30] The nuclease hypersensitive element (NHE) within the KRAS oncogene promoter contains several G-rich tracts capable of folding into G-quadruplex structures and represents a potential 'druggable' target for anticancer strategies, particularly considering that the K-ras protein has long been regarded as challenging to target pharmacologically by small molecule inhibitors due to the absence of a suitable hydrophobic pocket on its surface. [31] Within this framework, we focused on the G-rich KRAS22 oligonucleotide tract (5′-AGGGCGGTGTGGGAAGAGGGAA-3′), which engages in nuclear protein interactions and is involved in the transcriptional regulation of the KRAS gene. Because of the known structural polymorphism of the wild-type KRAS22 sequence, [32] in this study, we used its mutated KRAS22-RT analogue (5′-AGGGCGGTGTGGGAA**T**AGGGAA-3′) that folds into a single, well-defined parallel intramolecular GQ structure. [33,34] Seeking new natural ligands for KRAS22 G-quadruplexes, we assessed the binding potential of a small set of five secondary metabolites isolated from Mediterranean plants. The collection comprises three carexanes (**1**, **3** and **4**), isolated and characterized in-house and known for their antioxidant properties, [35,36] as well as the well-studied alkaloid magnoflorine (**2**), which is endowed with potent anti-inflammatory, antioxidant, and neuropsychopharmacological activities. [37,38] A multidisciplinary approach was employed to investigate the interaction of these compounds with the G-quadruplex structure formed by KRAS22-RT, integrating circular dichroism (CD) and nuclear magnetic resonance (NMR) analyses. Additionally, the in vitro anticancer activity of compounds **1–4** was evaluated in three breast cancer cell lines using a 3-(4,5-dimethylthiazol-2-yl)-5-(3-carboxymethoxyphenyl)-2-(4-sulfophenyl)-2*H*-tetrazolium (MTS) assay.

Table 1. Chemical structures of compounds **1–4**, and the Mediterranean plants from which they have been extracted.

Compound	Common name	Structure	Source	Reference
1	Distachyasin	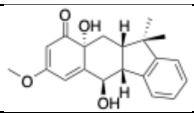	*Carex distachya*	[36]

 doi:10.20944/preprints202604.1302.v1

2	Magnoflorine	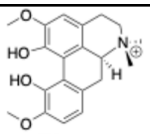	*Berberis cretica*	[37]
3	CxB	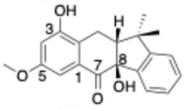	*Carex distachya*	[35]
4	CxC	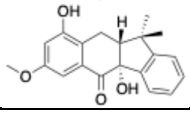	*Carex distachya*	[35]

2. Results and Discussion

2.1. Circular Dichroism (CD) Studies

Circular dichroism (CD) spectroscopy is a technique widely used to investigate the topology of GQ structures and to monitor conformational changes induced by ligand interactions. [39–44] In addition, CD melting experiments allow to evaluate the stability of these nucleic acid architectures in the presence of ligands. The CD spectrum of the KRAS22-RT GQ-forming sequence annealed in an 80 mM K^+ phosphate-buffered solution (pH = 7.0) displayed a positive band at 264 nm and a negative one at 244 nm (Figure 1), which confirmed the formation of the monomolecular parallel GQ structure previously reported by Yatsunik L.A et al., [33,45] whose melting temperature (T_M) was estimated as 52 °C, as assessed by determining the first derivative of the sigmoidal CD melting curve recorded at 264 nm (Figure 1A and Table 2). Prior to conducting the CD titration experiments, the aggregation behaviour of compounds **1–4** was examined through UV/Vis spectroscopy, by monitoring changes in absorbance at their λ_{max} upon incremental addition of the compounds to the phosphate-buffered solution (1–5 equivalents, steps of one, calculated with respect to the concentration of the single-stranded oligonucleotide). In all cases, aggregation could be ruled out, as a linear correlation was observed between absorbance and concentration across the entire concentration range tested (Figure S1, Supplementary Materials). Upon incubation of the KRAS22-RT GQ with increasing amounts of compounds **1–4**, the characteristic CD profile of the quadruplex structure was almost retained. Since chiral compounds **1–4** displayed weak CD signals within the same spectral region as the oligonucleotide sequence under investigation, their CD spectra were recorded at increasing concentrations (1–5 equiv.) under the same buffer and experimental conditions used for the titration assays (Figure S2). These reference spectra were then subtracted from the titration data to obtain only the actual contribution of the oligonucleotide–compound interactions. Thereafter, the CD_{264} melting curves, obtained upon incubation of KRAS22-RT GQ with 5 equiv. of each compound, were recorded, and the corresponding T_M values were extracted. For compound **1**, no effect on GQ stability was observed, as the calculated T_M value matched that of the GQ alone. By contrast, modest increases (2–3 °C) in T_M were detected for compounds **2** and **4**, indicating a slight stabilization of the GQ secondary structure. Notably, incubation of the GQ with compound **3** resulted in a marked stabilization, as evidenced by the 16 °C noteworthy increase in the T_M value, from 52 to 68 °C.

 doi:10.20944/preprints202604.1302.v1

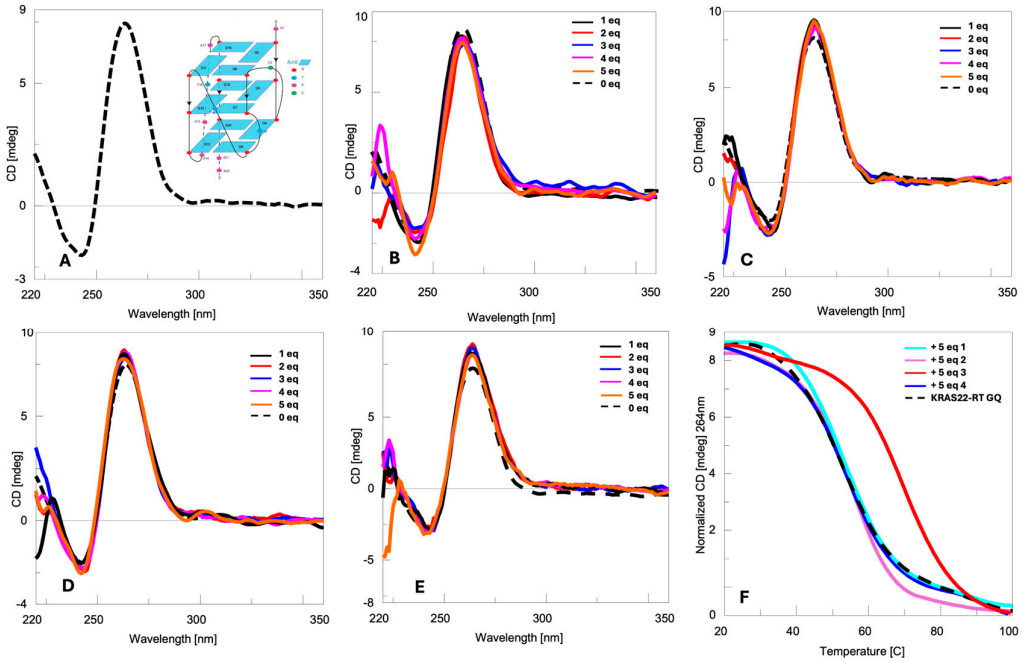

Figure 1. CD spectra of KRAS22-RT GQ in the absence (Panel A) and presence of increasing molar equivalents (1–5) of compounds **1** (Panel B), **2** (Panel C), **3** (Panel D) and **4** (Panel E). CD melting spectra of KRAS22-RT GQ in the absence and presence of 5 equiv. of compounds **1–4** (Panel F). CD spectra and CD melting curves were acquired in an 80 mmol/L K^+ phosphate-buffered solution (pH = 7.0). CD melting experiments were acquired by monitoring the normalized CD value of the higher positive Cotton effect in the temperature range 5–90 °C. In the insert of Panel A, a schematic representation of KRAS22-RT GQ is depicted. [33,34].

Table 2. Effects induced by the addition of 5 equiv. of compounds **1–4** on the CD profile and melting temperature of the KRAS22-RT G-quadruplex structure.

Entry	λ_{max} (nm)	λ_{min} (nm)	T_M (°C)	ΔT_M (°C) *
KRAS22-RT GQ	264	243	52	-
KRAS22-RT GQ + **1**	264	243	52	0
KRAS22-RT GQ + **2**	264	243	55	+3
KRAS22-RT GQ + **3**	264	243	68	+16
KRAS22-RT GQ + **4**	264	243	55	+3

* ΔT_M = T_M KRAS22-RT GQ + 5 equiv. of compound **1–4** − T_M KRAS22-RT GQ.

2.2. NMR Studies

To gain deeper insight into the structural features underlying the effect of the most interesting compound **3** on the KRAS22-RT GQ, ^{1}H NMR titration experiments were performed.[46–48] The single-stranded KRAS22-RT oligonucleotide was annealed in an 80 mM K^+ phosphate-buffered solution (pH = 7.0), and the corresponding KRAS22-RT GQ was investigated using water-suppressed ^{1}H NMR experiments (H_2O/D_2O, 9:1). [33,34] In accordance with the literature data, [32] KRAS22-RT GQ showed twelve proton signals in the range 12.0–10.6 ppm corresponding to the exchange-protected N^1 imino protons of the twelve guanines forming the three stacked G-tetrads. Upon titration with 1–5 equivalents of compound **3**, the GQ imino proton region showed no additional resonances beyond those present in the free GQ structure. Interestingly, the progressive addition of compound **3** resulted in small up-field chemical shift perturbations for all monitored imino resonances. This latter behavior is characteristic of a fast exchange on the NMR timescale between the free G-quadruplex and the ligand-bound complex, indicating rapid association and dissociation kinetics relative to the difference in chemical shift frequencies between the two states, and the absence

 doi:10.20944/preprints202604.1302.v1

of long-lived, structurally distinct bound states. [49]. The observed chemical-shift changes were modest and displayed a comparable trend among all the different imino protons. The chemical shift variations (Dd) upon addition of increasing amounts of compound **3** followed a smooth and saturable profile, reaching a plateau at higher ligand equivalents (Figure S3).

Since compound **3** does not possess structural features typically associated with intercalation or end-stacking onto terminal G-quartets, [50–54] the observed smooth and uniform up-field shifts of the imino proton resonances could be rationalized in terms of external bindings, [40,55,56] as also proposed for other KRAS G-quadruplex ligands. [34]

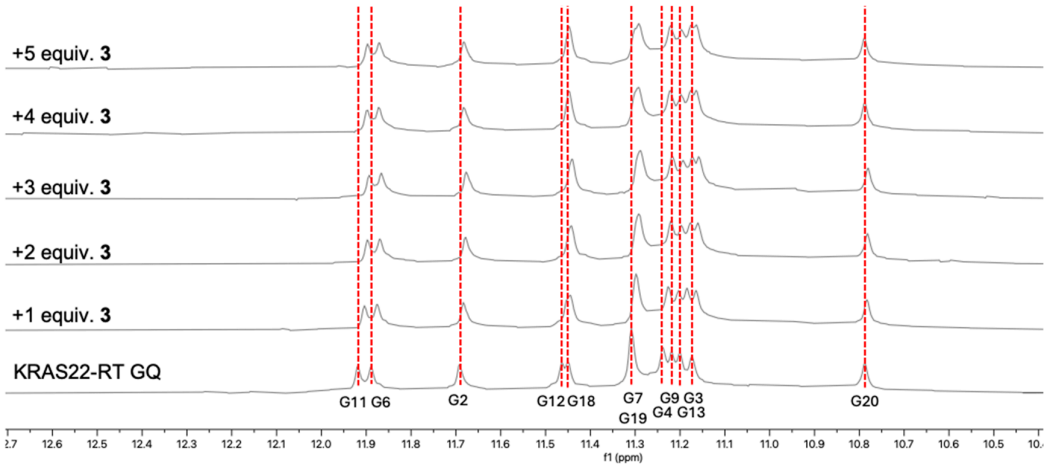

Figure 2. Expansion of the imino regions of the water-suppressed ^{1}H NMR spectra (H_2O/D_2O, 9:1) of KRAS22-RT GQ annealed in 80 mM K^+ phosphate-buffered solution recorded at 25 °C before and after the addition of 1–5 equiv. of compound **3**.

The thermal stability of the KRAS22-RT GQ + **3** complex was evaluated by monitoring the intensity of imino proton signals at increasing temperatures (25–75 °C, steps of ten), following incubation of KRAS22-RT GQ with 5 equiv. of compound **3**. The imino signals progressively decreased with rising temperature and disappeared completely between 65 and 75 °C, in agreement with the CD melting data (Figure S4). Interestingly, upon cooling the sample back to 25 °C, the KRAS22-RT GQ was restored, displaying that compound **3** did not interfere with the re-formation of the secondary structure. This behavior suggests that compound **3** might act as a transient GQ-stabilizing agent, promoting structural integrity under stress conditions (e.g., thermal denaturation) without permanently locking the nucleic acid into a rigid conformation. Such a feature could be advantageous in a biological context, where dynamic regulation of GQ folding/unfolding is required for the transcriptional control.

In contrast to compound **3**, its diastereomer **4**, bearing the opposite absolute configuration at the C-8 position, displayed only a marginal stabilizing effect on the GQ structure, as evidenced by a modest increase in melting temperature (ΔT_M = + 2 °C). However, ^{1}H NMR titration experiments (Figure S5) of KRAS22-RT GQ with compound **4** (1–5 equiv.) revealed distinct perturbation patterns in the imino proton chemical shifts compared to compound **3** (Figure S6). In detail, compound **4** induced much larger chemical-shift perturbations already at one equivalent added, followed by a partial decrease or redistribution of the shifts upon further addition of compound **4**, and then by a more limited variation at higher equivalents. This behavior suggested the presence of an initial high-affinity interaction, followed by structural rearrangement and/or weaker secondary binding events. The more pronounced perturbations observed for G2, G4, and G6 imino protons after the addition of the first equivalent of compound **4** could be rationalized by the spatial arrangement of the corresponding guanine residues on the same lateral face of the GQ, suggesting that compound **4** preferentially interacted with this exposed surface region. Despite a stronger observed NMR

 doi:10.20944/preprints202604.1302.v1

response, the interaction of compound **4** with KRAS22-RT GQ was much less effective in stabilizing the GQ core with respect to compound **3**. The different stability of the folded state observed upon interaction with compound **3** may highlight the critical role of C-8 stereochemistry and the resulting differences in the three-dimensional arrangement of functional groups in governing a productive GQ recognition.

Similarly to compound **3**, the thermal stability of the KRAS22-RT GQ in the presence of compound **4** was assessed by monitoring the temperature-dependent decay of the imino proton signals after incubation with 5 equiv. of compound **4**. A progressive signal loss was observed upon heating, with complete disappearance between 55 and 65 °C, in agreement with the CD melting data. As observed for compound **3**, the KRAS22-RT GQ was restored upon cooling the sample back to 25 °C, indicating that compound **4** also did not hinder the re-formation of the secondary structure (Figure S7).

2.3. Evaluation of the Antiproliferative Activity of Compounds 1–4

The cytotoxic activity of compounds **1–4** was evaluated in three breast cancer cell lines using an MTS assay after 72 h of treatment. The IC_{50} values are reported in Table 3. Notably, some compounds exhibited markedly lower IC_{50} values in the resistant cell line compared to the parental one. This observation, although uncommon, warrants further investigation to determine whether these compounds may modulate specific targets and induce a phenomenon known as "collateral sensitivity". Notably, compound **4** showed the strongest activity in the normal HMEpiC line, with an IC_{50} below 10 μg/mL, suggesting limited selectivity.

Table 3. IC_{50} values after 72 h of treatment with compounds **1–4** in three breast cancer cell lines (MCF-7, MCF7-R and MDA-MB-231) and in one normal cell line (HMEpiC).

	MCF-7 IC_{50} (μg/mL) ± SE	MCF-7R IC_{50} (μg/mL) ± SE	MDA-MB-231 IC_{50} (μg/mL) ± SE	HMEpiC IC_{50} (μg/mL) ± SE
1	38.5 ± 2.2	17.3 ± 1.1	24.3 ± 3.1	26.2 ± 0.9
2	39.2 ± 6.9	30.7 ± 2.3	28.5 ± 1.2	20.0 ± 0.0
3	28.3 ± 1.8	16.7 ± 0.6	22.5 ± 3.2	14.0 ± 0.7
4	28.7 ± 1.5	13.3 ± 0.7	25.7 ± 1.8	< 10.0

3. Materials and Methods

3.1. Preparation of Oligonucleotide KRAS-22RT

The oligonucleotide KRAS-22RT was prepared by solid-phase synthesis using the β-cyanoethyl phosphoramidite chemistry on a Expedite 8909 DNA synthesizer. The standard monomers were assembled over a CPG Universal Support (35 mg, 1.4 μmol) using a 1 μmol scale protocol. The oligonucleotide was detached from the solid support and deprotected by an aqueous ammonia solution treatment at 55 °C for 12 h. The combined filtrates and washings were collected and evaporated under reduced pressure. The crude sample was dissolved in H_2O, purified by HPLC on a Jasco PU-4180 Plus instrument equipped with a Jasco UV-4075 Plus UV detector (Jasco Europe s.r.l., Milan, Italy) using a Nucleogel® SAX 1000–8 strong anion exchange column (Macherey-Nagel, Duren, Germany) eluted with a linear gradient of 1 M NaCl and 20 mM NaH_2PO_4 aqueous solution (pH = 7.0) containing 20% (v/v) CH_3CN in H_2O (from 0 to 100% in 45 min., flow rate of 1.0 mL/min.) and desalted on a Biogel-P2 column (Bio-Rad Laboratories s.r.l., Segrate, Italy). The structure of the oligonucleotide was confirmed by ESI MS analyses. Oligonucleotide concentration was determined spectrophotometrically at λ = 260 nm and 90 °C, using the molar extension coefficient ε = 233.1 cm^{-1} L mol^{-1}, as calculated using the Sigma-Aldrich OligoEvaluatorTM web tool (www.oligoevaluator.com, accessed on 5 September 2024).

 doi:10.20944/preprints202604.1302.v1

3.2. Preparation of KRAS-22RT GQ

The GQ was prepared by dissolving the lyophilized single stranded oligonucleotide in 80 mM potassium phosphate buffered solution (60 mM KCl, 20 mM KH_2PO_4, pH 7.0). The solution was heated at 90 °C for 5 min, and slowly cooled to 25 °C. The annealing procedures were followed by overnight storage at 4 °C prior to use.

3.3. Circular Dichroism (CD) Experiments

CD spectra were recorded on a Jasco J-1400 spectropolarimeter (JASCO Inc., Tokyo, Japan) equipped with a Peltier temperature controller. All the spectra were recorded at 25 °C in the 220–500 nm wavelength range and averaged over three scans. The scan rate was 100 nm min^{-1}, with a 4 sec response and 1 nm bandwidth. Buffer baseline was subtracted from each spectrum. CD spectra of GQ + compounds **1–4** were obtained by adding increasing amounts of compounds **1–4** (1–5 equiv., step of 1) dissolved in CH_3OH (0.4%). [57] The contribution of each compound was subtracted from each spectrum. The CD spectra were acquired after a 10 min incubation time. The CD melting experiments were performed by monitoring the CD value of the higher positive Cotton effect in the temperature range of 20–90 °C at the 0.5 °C/min heating rate after incubation of GQ with 5 equiv. of compounds **1–4**.

3.4. NMR Titration and Melting Experiments

NMR spectra were acquired on Bruker Avance Neo 600 MHz spectrometers (Bruker-Biospin). One-dimensional ^1H NMR spectra were acquired as 16,384 data points with a recycle delay of 1.0 s at 25 °C, and the spectra were apodized with a shifted sine bell squared window function. Water suppression was achieved by including a double pulsed-field gradient spin-echo (DPFGSE) module in the pulse sequence prior to acquisition. The NMR spectra were processed using the MestReNova (version 14.3.0, Mestrelab Research, Santiago de Compostela, Spain) suite. NMR spectra were acquired at 0.52 mM single stranded oligonucleotide concentration in 80 mM phosphate buffered solution (60 mM KCl, 20 mM KH_2PO_4, pH 7.0; H_2O/D_2O, 9:1, v/v) pH 7.0. Compounds **3** and **4** were dissolved in CD_3OD and added to KRAS-22RT GQ (1–5 equiv., final CD_3OD concentration 0.4%). [57] After addition of each compound, the solution was equilibrated for 10 min at 25 °C before spectra acquisition. ^1H NMR melting experiments (25, 35, 45, 55, 65 and 75 °C) were performed after incubation of KRAS-22RT GQ with 5 equiv. of compounds **3** and **4**, with an equilibration time of 10 min at each temperature.

3.5. Cell Lines and Culture Conditions

Human MCF-7 breast adenocarcinoma cells and MDA-MB-231 triple-negative breast cancer cells were obtained from ATCC (HTB-22™ and HTB-26™, Rockville, MD, USA, respectively). The multidrug-resistant (MDR) MCF-7R cell line was established by exposing parental MCF-7 cells to sub-cytotoxic concentrations of doxorubicin. The IC_{50} of doxorubicin in MCF-7R cells is approximately 75-fold higher than that in parental cells. MCF-7R cells lack ERα expression and are insensitive to estrogen stimulation. In addition, they show constitutive activation of the NF-κB pathway and overexpression of NF-κB target proteins, including Inhibitor of Apoptosis Proteins (IAPs) and P-glycoprotein, contributing to resistance to multiple antineoplastic agents. Cells were cultured in DMEM supplemented with 10% heat-inactivated FBS, 2 mM L-glutamine, 100 U/mL penicillin, and 100 μg/mL streptomycin. The normal human mammary epithelial cell line HMEpiC (Innoprot, P10891, Derio, Spain) was used as a non-tumorigenic control and cultured in Mammary Epithelial Cell Medium supplemented with Mammary Epithelial Cell Growth Supplement and penicillin/streptomycin solution (Innoprot). All cell lines were maintained at 37 °C in an humidified atmosphere with 5% CO_2. Cells within a narrow passage range were used for all experiments. Cultures were maintained as adherent monolayers in complete medium and routinely tested for Mycoplasma contamination before use.

 doi:10.20944/preprints202604.1302.v1

3.6. Cell Proliferation Assay

Cell proliferation was evaluated under the culture conditions described above. Cells were seeded in 96-well plates at a density of 5×10^3 cells/well and allowed to adhere overnight at 37 °C. At time zero, the medium was replaced with fresh complete medium containing the tested compounds **1–4** at the indicated concentrations. After 72 h of treatment, 16 µL of a commercial MTS solution (Promega Corporation, Madison, WI, USA), containing 3-(4,5-dimethylthiazol-2-yl)-5-(3-carboxymethoxyphenyl)-2-(4-sulfophenyl)-2*H*-tetrazolium and phenazine ethosulfate, was added to each well. Plates were incubated for 2 h at 37 °C in a humidified atmosphere with 5% CO_2. Cell viability was determined by measuring the absorbance at 490 nm using a microplate reader (iMark Microplate Reader; Bio-Rad Laboratories, Inc., Hercules, CA, USA). Cell growth inhibition was expressed as a percentage relative to untreated control cells and reported as mean ± standard error (SE).

4. Conclusions

In this study, we evaluated the ligand properties of compounds **1–4**, extracted from the Mediterranean plants *Carex distachya* and *Berberis cretica*, towards the KRAS22-RT GQ, a modified KRAS-derived oligonucleotide commonly used as a model of the KRAS oncogene. Among the tested molecules, compound **3** proved to be the most effective, markedly increasing the thermal stability of the GQ. NMR data indicated that compound **3** interacted with the GQ in a fast exchange regime, consistent with an external binding mode. The comparison with its C-8 diastereomer (compound **4**) highlighted the critical role of stereochemistry at that position in GQ stabilization. Notably, compound **3** combines a strong GQ stabilization with a significant antiproliferative activity in both sensitive and drug-resistant breast cancer cell lines, suggesting a promising pharmacological profile. However, further studies are required to elucidate its precise mechanism of action and to clarify whether the observed biological effects are directly linked to KRAS gene modulation via GQ formation/stabilization. Overall, our work expands the current understanding of how natural scaffolds can be exploited to selectively recognize and stabilize GQ structures, reinforcing the value of natural products as a source of bioactive molecules. These findings provide a basis for future investigations into GQ-targeted therapeutics and support the development of innovative anticancer strategies based on the modulation of non-canonical DNA architectures. In this context, compound **3** emerges as a promising lead for the rational design of more potent GQ-targeting agents.

Supplementary Materials: The following supporting information can be downloaded at the website of this paper posted on Preprints.org, Figure S1: UV titration spectra of compounds **1–4**; Figure S2: CD titration spectra of compounds **1–4**; Figure S3: Compound **3**–induced shift changes in KRAS22-RT GQ **4**; Figure S4: NMR thermal stability of KRAS22-RT GQ with compound **3**; Figure S5: NMR titration experiment of KRAS22-RT GQ with compound **4**; Figure S6: Compound **4**–induced shift changes in KRAS22-RT GQ; Figure S7: NMR thermal stability of KRAS22-RT GQ with compound **4**; Figures S8–S11: Copies of ^{1}H NMR spectra of compounds **1–4**.

Author Contributions: Conceptualization, S.R., A.F., S.D.E., N.B.; methodology and design, S.D., N.B.; methodology and isolation of natural products, A.F., G.V., M.S., B.D.A.; physico-chemical characterization and data analysis, M.M., M.G.N., C.P., G.V.; biological experiments and data analysis, M.N., P.P.; writing—original draft preparation, S.D.; writing— review and editing, S.R., A.F., S.D., N.B.; funding acquisition, S.R., A.F., N.B. All authors have read and agreed to the published version of the manuscript.

Funding: This research was funded by PRIN 2022 PNRR project "Small Molecule Anticancer Ligands Library from Mediterranean Plants (SMALL)" code: P2022YJZ5F – CUP E53D23016150001 and by BANDYT project "A breakthrough plasmonic nanosensor for the point-of-care detection of acute myocardial stroke biomarkers" code: FISA-2024-00069.

Institutional Review Board Statement: Not applicable.

Informed Consent Statement: Not applicable.

 doi:10.20944/preprints202604.1302.v1

Data Availability Statement: Data are contained within the article and Supplementary Materials.

Acknowledgments: The authors are grateful to Luisa Cuorvo for the technical assistance.

Conflicts of Interest: The authors declare no conflicts of interest.

Abbreviations

The following abbreviations are used in this manuscript:

ATCC / American Type Culture Collection
CD — Circular Dichroism
CH_3CN — Acetonitrile
CH_3OH / CD_3OD — Methanol / Deuterated methanol
CO_2 — Carbon dioxide
CPG — Controlled Pore Glass
CxB / CxC — Carexane derivatives from *Carex distachya*
DMEM — Dulbecco's Modified Eagle Medium
DNA — Deoxyribonucleic Acid
DPFGSE — Double Pulsed-Field Gradient Spin-Echo
ERα — Estrogen Receptor alpha
ESI MS — Electrospray Ionization Mass Spectrometry
FBS — Fetal Bovine Serum
GQ / GQs — G-Quadruplex / G-Quadruplexes
H_2O / D_2O — Water / Deuterated water
HMEpiC — Human Mammary Epithelial Cells
HPLC — High-Performance Liquid Chromatography
IAPs — Inhibitor of Apoptosis Proteins
IC_{50} — Half maximal inhibitory concentration
KRAS — Kirsten Rat Sarcoma viral oncogene homolog
KRAS22 — G-rich oligonucleotide sequence of KRAS promoter
KRAS22-RT — Mutated variant of KRAS22 sequence
KCl — Potassium chloride
KH_2PO_4 — Potassium dihydrogen phosphate
MAPK — Mitogen-Activated Protein Kinase
MDR — Multidrug Resistance
MCF-7 — Human breast cancer cell line
MCF-7R — Drug-resistant variant of MCF-7
MDA-MB-231 — Triple-negative breast cancer cell line
MTS — 3-(4,5-dimethylthiazol-2-yl)-5-(3-carboxymethoxyphenyl)-2-(4-sulfophenyl)-2*H*-tetrazolium
NaCl — Sodium chloride
NaH_2PO_4 — Sodium dihydrogen phosphate
NHE — Nuclease Hypersensitive Element
NMR — Nuclear Magnetic Resonance
PI3K — Phosphoinositide 3-kinase
RNA — Ribonucleic Acid
SAX — Strong Anionic Exchange
SE — Standard Error
T_M — Melting Temperature
UV/Vis — Ultraviolet-Visible spectroscopy

 doi:10.20944/preprints202604.1302.v1

References

1. Barbieri, F.; Tabanelli, G.; Braschi, G.; Bassi, D.; Morandi, S.; Šimat, V.; Čagalj, M.; Gardini, F.; Montanari, C. Mediterranean Plants and Spices as a Source of Bioactive Essential Oils for Food Applications: Chemical Characterisation and In Vitro Activity. *Int. J. Mol. Sci.* **2025**, *26*, 3875, doi:10.3390/ijms26083875.
2. Chileh-Chelh, T.; Ezzaitouni, M.; Belarbi, E.-H.; Guil-Guerrero, J.L. Mediterranean Wild Edible Plants as Promising Sources of Less-Polar Bioactive Compounds: Fatty Acids, Carotenoids, Tocopherols, and Sterols. *Journal of Food Composition and Analysis* **2025**, *148*, 108370, doi:10.1016/j.jfca.2025.108370.
3. Vella, F.M.; Pignone, D.; Laratta, B. The Mediterranean Species Calendula Officinalis and Foeniculum Vulgare as Valuable Source of Bioactive Compounds. *Molecules* **2024**, *29*, 3594, doi:10.3390/molecules29153594.
4. Gao, L.; Liu, X.; Luo, X.; Lou, X.; Li, P.; Li, X.; Liu, X. Antiaging Effects of Dietary Supplements and Natural Products. *Front. Pharmacol.* **2023**, *14*, doi:10.3389/fphar.2023.1192714.
5. Bjørklund, G.; Shanaida, M.; Lysiuk, R.; Butnariu, M.; Peana, M.; Sarac, I.; Strus, O.; Smetanina, K.; Chirumbolo, S. Natural Compounds and Products from an Anti-Aging Perspective. *Molecules* **2022**, *27*, 7084, doi:10.3390/molecules27207084.
6. Latif, R.; Nawaz, T. Medicinal Plants and Human Health: A Comprehensive Review of Bioactive Compounds, Therapeutic Effects, and Applications. *Phytochemistry Reviews* **2026**, *25*, 2299–2342, doi:10.1007/s11101-025-10194-7.
7. Twaij, B.M.; Hasan, Md.N. Bioactive Secondary Metabolites from Plant Sources: Types, Synthesis, and Their Therapeutic Uses. *International Journal of Plant Biology* **2022**, *13*, 4–14, doi:10.3390/ijpb13010003.
8. Aware, C.B.; Patil, D.N.; Suryawanshi, S.S.; Mali, P.R.; Rane, M.R.; Gurav, R.G.; Jadhav, J.P. Natural Bioactive Products as Promising Therapeutics: A Review of Natural Product-Based Drug Development. *South African Journal of Botany* **2022**, *151*, 512–528, doi:10.1016/j.sajb.2022.05.028.
9. Wang, K.-B.; Wang, Y.; Dickerhoff, J.; Yang, D. DNA G-Quadruplexes as Targets for Natural Product Drug Discovery. *Engineering* **2024**, *38*, 39–51, doi:10.1016/j.eng.2024.03.015.
10. Mazzini, S.; Princiotto, S.; Musso, L.; Passarella, D.; Beretta, G.L.; Perego, P.; Dallavalle, S. Synthesis and Investigation of the G-Quadruplex Binding Properties of Kynurenic Acid Derivatives with a Dihydroimidazoquinoline-3,5-Dione Core. *Molecules* **2022**, *27*, 2791, doi:10.3390/molecules27092791.
11. Marzano, M.; Nolli, M.G.; D'Errico, S.; Falanga, A.P.; Terracciano, M.; Dardano, P.; De Stefano, L.; Piccialli, G.; Borbone, N.; Oliviero, G. Enhancing G-Quadruplex-Based DNA Nanotechnology: New Lipophilic DNA G-Quadruplexes with TBDPS Modifications. *RSC Adv.* **2025**, *15*, 17933–17945, doi:10.1039/D5RA01033K.
12. Spiegel, J.; Adhikari, S.; Balasubramanian, S. The Structure and Function of DNA G-Quadruplexes. *Trends Chem.* **2020**, *2*, 123–136, doi:10.1016/j.trechm.2019.07.002.
13. Lam, E.Y.N.; Beraldi, D.; Tannahill, D.; Balasubramanian, S. G-Quadruplex Structures Are Stable and Detectable in Human Genomic DNA. *Nat. Commun.* **2013**, *4*, doi:10.1038/ncomms2792.
14. Kosiol, N.; Juranek, S.; Brossart, P.; Heine, A.; Paeschke, K. G-Quadruplexes: A Promising Target for Cancer Therapy. *Mol. Cancer* **2021**, *20*, 40, doi:10.1186/s12943-021-01328-4.
15. Xu, J.; Huang, H.; Zhou, X. G-Quadruplexes in Neurobiology and Virology: Functional Roles and Potential Therapeutic Approaches. *JACS Au* **2021**, *1*, 2146–2161, doi:10.1021/jacsau.1c00451.
16. Yan, M.P.; Wee, C.E.; Yen, K.P.; Stevens, A.; Wai, L.K. G-Quadruplex Ligands as Therapeutic Agents against Cancer, Neurological Disorders and Viral Infections. *Future Med. Chem.* 2023, *15*, 1987–2009.
17. Xu, Y.; Komiyama, M. G-Quadruplexes in Human Telomere: Structures, Properties, and Applications. *Molecules* **2023**, *29*, 174, doi:10.3390/molecules29010174.
18. Falanga, A.P.; Piccialli, I.; Greco, F.; D'Errico, S.; Nolli, M.G.; Borbone, N.; Oliviero, G.; Roviello, G.N. Nanostructural Modulation of G-Quadruplex in Neurodegeneration: Orotate Interaction Revealed Through Experimental and Computational Approaches. *J. Neurochem.* **2025**, *169*, doi:10.1111/jnc.16296.
19. Platella, C.; Ghirga, F.; Zizza, P.; Pompili, L.; Marzano, S.; Pagano, B.; Quaglio, D.; Vergine, V.; Cammarone, S.; Botta, B.; et al. Identification of Effective Anticancer G-Quadruplex-Targeting Chemotypes through the Exploration of a High Diversity Library of Natural Compounds. *Pharmaceutics* **2021**, *13*, 1611, doi:10.3390/pharmaceutics13101611.

 doi:10.20944/preprints202604.1302.v1

20. Chen, J.; He, Y.; Xu, Y.; Umer, M.; Anwar, N.; Wei, S.; Liu, W.; Wang, Z.; Gao, C. Higher Selective Targeting of Telomeric Multimeric G-Quadruplex by Natural Product Berberine. *Curr. Med. Chem.* **2026**, *33*, 676–688, doi:10.2174/0109298673345414241202094409.
21. Das, A.; Dutta, S. Binding Studies of Aloe-Active Compounds with G-Quadruplex Sequences. *ACS Omega* **2021**, *6*, 18344–18351, doi:10.1021/acsomega.1c02207.
22. Pirota, V.; Stasi, M.; Benassi, A.; Doria, F. An Overview of Quadruplex Ligands: Their Common Features and Chemotype Diversity. In *Annual Reports in Medicinal Chemistry*; Academic Press Inc., 2020; Vol. 54, pp. 163–196.
23. Zhang, H.; Xiang, J.; Hu, H.; Liu, Y.; Yang, F.; Shen, G.; Tang, Y.; Chen, C. Selective Recognition of Specific G-Quadruplex vs. Duplex DNA by a Phenanthroline Derivative. *Int. J. Biol. Macromol.* **2015**, *78*, 149–156, doi:10.1016/j.ijbiomac.2015.03.034.
24. Hashimoto, Y.; Imagawa, Y.; Nagano, K.; Maeda, R.; Nagahama, N.; Torii, T.; Kinoshita, N.; Takamiya, N.; Kawauchi, K.; Tatesishi-Karimata, H.; et al. Simple and Fast Screening for Structure-Selective G-Quadruplex Ligands. *Chemical Communications* **2023**, *59*, 4891–4894, doi:10.1039/D3CC00556A.
25. Asamitsu, S.; Obata, S.; Yu, Z.; Bando, T.; Sugiyama, H. Recent Progress of Targeted G-Quadruplex-Preferred Ligands Toward Cancer Therapy. *Molecules* **2019**, *24*, 429, doi:10.3390/molecules24030429.
26. Choucair, K.; Imtiaz, H.; Uddin, M.H.; Nagasaka, M.; Al-Hallak, M.N.; Philip, P.A.; El-Rayes, B.; Pasche, B.C.; Azmi, A.S. Targeting KRAS Mutations: Orchestrating Cancer Evolution and Therapeutic Challenges. *Signal Transduct. Target. Ther.* **2025**, *10*, 385, doi:10.1038/s41392-025-02473-8.
27. Uniyal, P.; Kashyap, V.K.; Behl, T.; Parashar, D.; Rawat, R. KRAS Mutations in Cancer: Understanding Signaling Pathways to Immune Regulation and the Potential of Immunotherapy. *Cancers (Basel).* **2025**, *17*, 785, doi:10.3390/cancers17050785.
28. Hyman, D.M.; Taylor, B.S.; Baselga, J. Implementing Genome-Driven Oncology. *Cell* **2017**, *168*, 584–599, doi:10.1016/j.cell.2016.12.015.
29. Lefort, S.; Tan, S.; Balani, S.; Rafn, B.; Pellacani, D.; Hirst, M.; Sorensen, P.H.; Eaves, C.J. Initiation of Human Mammary Cell Tumorigenesis by Mutant KRAS Requires YAP Inactivation. *Oncogene* **2020**, *39*, 1957–1968, doi:10.1038/s41388-019-1111-0.
30. Singh, A.; Greninger, P.; Rhodes, D.; Koopman, L.; Violette, S.; Bardeesy, N.; Settleman, J. A Gene Expression Signature Associated with "K-Ras Addiction" Reveals Regulators of EMT and Tumor Cell Survival. *Cancer Cell* **2009**, *15*, 489–500, doi:10.1016/j.ccr.2009.03.022.
31. Cox, A.D.; Fesik, S.W.; Kimmelman, A.C.; Luo, J.; Der, C.J. Drugging the Undruggable RAS: Mission Possible? *Nat. Rev. Drug Discov.* **2014**, *13*, 828–851, doi:10.1038/nrd4389.
32. Ou, A.; Schmidberger, J.W.; Wilson, K.A.; Evans, C.W.; Hargreaves, J.A.; Grigg, M.; O'Mara, M.L.; Iyer, K.S.; Bond, C.S.; Smith, N.M. High Resolution Crystal Structure of a KRAS Promoter G-Quadruplex Reveals a Dimer with Extensive Poly-A π-Stacking Interactions for Small-Molecule Recognition. *Nucleic Acids Res.* **2020**, *48*, 5766–5776, doi:10.1093/NAR/GKAA262.
33. Kerkour, A.; Marquevielle, J.; Ivashchenko, S.; Yatsunyk, L.A.; Mergny, J.L.; Salgado, G.F. High-Resolution Three-Dimensional NMR Structure of the KRAS Proto-Oncogene Promoter Reveals Key Features of a G-Quadruplex Involved in Transcriptional Regulation. *Journal of Biological Chemistry* **2017**, *292*, 8082–8091, doi:10.1074/jbc.M117.781906.
34. Wang, X.D.; Nie, Q.W.; Hu, M.H. A Small-Sized Imidazole-Derived Ligand Binds to the KRAS Promoter G-Quadruplex and Inhibits Cancer Growth with Enhanced Immunomodulation. *Journal of Biological Chemistry* **2025**, *301*, doi:10.1016/j.jbc.2025.110647.
35. Fiorentino, A.; D'Abrosca, B.; Pacifico, S.; Iacovino, R.; Izzo, A.; Uzzo, P.; Russo, A.; Di Blasio, B.; Monaco, P. Carexanes from Carex Distachya Desf.: Revised Stereochemistry and Characterization of Four Novel Polyhydroxylated Prenylstilbenes. *Tetrahedron* **2008**, *64*, 7782–7786, doi:10.1016/j.tet.2008.05.137.
36. Fiorentino, A.; D'Abrosca, B.; Pacifico, S.; Iacovino, R.; Mastellone, C.; Di Blasio, B.; Monaco, P. Distachyasin: A New Antioxidant Metabolite from the Leaves of Carex Distachya. *Bioorg. Med. Chem. Lett.* **2006**, *16*, 6096–6101, doi:10.1016/j.bmcl.2006.08.106.
37. Okon, E.; Kukula-Koch, W.; Halasa, M.; Jarzab, A.; Baran, M.; Dmoszynska-Graniczka, M.; Angelis, A.; Kalpoutzakis, E.; Guz, M.; Stepulak, A.; et al. Magnoflorine—Isolation and the Anticancer Potential against

 doi:10.20944/preprints202604.1302.v1

NCI-H1299 Lung, MDA-MB-468 Breast, T98G Glioma, and TE671 Rhabdomyosarcoma Cancer Cells. *Biomolecules* **2020**, *10*, 1532, doi:10.3390/biom10111532.

38. Xu, T.; Kuang, T.; Du, H.; Li, Q.; Feng, T.; Zhang, Y.; Fan, G. Magnoflorine: A Review of Its Pharmacology, Pharmacokinetics and Toxicity. *Pharmacol. Res.* **2020**, *152*, 104632, doi:10.1016/j.phrs.2020.104632.
39. del Villar-Guerra, R.; Trent, J.O.; Chaires, J.B. G-Quadruplex Secondary Structure Obtained from Circular Dichroism Spectroscopy. *Angewandte Chemie* **2018**, *130*, 7289–7293, doi:10.1002/ange.201709184.
40. Marzano, M.; Prencipe, F.; Delre, P.; Mangiatordi, G.F.; Travagliante, G.; Ronga, L.; Piccialli, G.; Saviano, M.; D'Errico, S.; Tesauro, D.; et al. A CD Study of a Structure-Based Selection of N-Heterocyclic Bis-Carbene Gold(I) Complexes as Potential Ligands of the G-Quadruplex-Forming Human Telomeric HTel23 Sequence. *Molecules* **2024**, *29*, 5446, doi:10.3390/molecules29225446.
41. Carvalho, J.; Queiroz, J.A.; Cruz, C. Circular Dichroism of G-Quadruplex: A Laboratory Experiment for the Study of Topology and Ligand Binding. *J. Chem. Educ.* **2017**, *94*, 1547–1551, doi:10.1021/acs.jchemed.7b00160.
42. Falanga, A.P.; D'Urso, A.; Travagliante, G.; Gangemi, C.M.A.; Marzano, M.; D'Errico, S.; Terracciano, M.; Greco, F.; De Stefano, L.; Dardano, P.; et al. Higher-Order G-Quadruplex Structures and Porphyrin Ligands: Towards a Non-Ambiguous Relationship. *Int. J. Biol. Macromol.* **2024**, *268*, 131801, doi:10.1016/j.ijbiomac.2024.131801.
43. Fracchioni, G.; Vailati, S.; Grazioli, M.; Pirota, V. Structural Unfolding of G-Quadruplexes: From Small Molecules to Antisense Strategies. *Molecules* **2024**, *29*, 3488, doi:10.3390/molecules29153488.
44. Santos, T.; Salgado, G.F.; Cabrita, E.J.; Cruz, C. G-Quadruplexes and Their Ligands: Biophysical Methods to Unravel G-Quadruplex/Ligand Interactions. *Pharmaceuticals* **2021**, *14*, 769, doi:10.3390/ph14080769.
45. D'Aria, F.; Pagano, B.; Petraccone, L.; Giancola, C. KRAS Promoter G-Quadruplexes from Sequences of Different Length: A Physicochemical Study. *Int. J. Mol. Sci.* **2021**, *22*, 448, doi:10.3390/ijms22010448.
46. Dickerhoff, J.; Yang, D. NMR Structure Study of DNA G-Quadruplexes and Ligand Complexes. *Prog. Nucl. Magn. Reson. Spectrosc.* **2026**, *154–155*, 101597, doi:10.1016/j.pnmrs.2026.101597.
47. Marzano, M.; D'Errico, S.; Greco, F.; Falanga, A.P.; Terracciano, M.; Di Prisco, D.; Piccialli, G.; Borbone, N.; Oliviero, G. Polymorphism of G-Quadruplexes Formed by Short Oligonucleotides Containing a 3′-3′ Inversion of Polarity: From G:C:G:C Tetrads to π–π Stacked G-Wires. *Int. J. Biol. Macromol.* **2023**, *253*, 127062, doi:10.1016/j.ijbiomac.2023.127062.
48. Marzano, M.; Falanga, A.P.; Dardano, P.; D'Errico, S.; Rea, I.; Terracciano, M.; De Stefano, L.; Piccialli, G.; Borbone, N.; Oliviero, G. π–π Stacked DNA G-Wire Nanostructures Formed by a Short G-Rich Oligonucleotide Containing a 3′–3′ Inversion of Polarity Site. *Organic Chemistry Frontiers* **2020**, *7*, 2187–2195, doi:10.1039/D0QO00561D.
49. Reed, C.R.; Kennedy, S.D.; Horowitz, R.H.; Keedakkatt Puthenpeedikakkal, A.M.; Stern, H.A.; Mathews, D.H. Modeling and NMR Data Elucidate the Structure of a G-Quadruplex-Ligand Interaction for a Pu22T-Cyclometalated Iridium(III) System. *Journal of Physical Chemistry B* **2024**, *128*, 11634–11643, doi:10.1021/acs.jpcb.4c06262.
50. Wang, K.-B.; Liu, Y.; Li, J.; Xiao, C.; Wang, Y.; Gu, W.; Li, Y.; Xia, Y.-Z.; Yan, T.; Yang, M.-H.; et al. Structural Insight into the Bulge-Containing KRAS Oncogene Promoter G-Quadruplex Bound to Berberine and Coptisine. *Nat. Commun.* **2022**, *13*, 6016, doi:10.1038/s41467-022-33761-4.
51. Coban, T.; Robertson, C.; Schwikkard, S.; Singer, R.; Legresley, A. Synthesis and Evaluation of Bis(Imino)Anthracene Derivatives as G-Quadruplex Ligands. *RSC Med. Chem.* **2021**, *12*, 751–757, doi:10.1039/d0md00428f.
52. Dallavalle, S.; Musso, L.; Artali, R.; Aviñó, A.; Scaglioni, L.; Eritja, R.; Gargallo, R.; Mazzini, S. G-Quadruplex Binding Properties of a Potent PARP-1 Inhibitor Derived from 7-Azaindole-1-Carboxamide. *Sci. Rep.* **2021**, *11*, doi:10.1038/s41598-021-83474-9.
53. Carvalho, J.; Pereira, E.; Marquevielle, J.; Campello, M.P.C.; Mergny, J.-L.; Paulo, A.; Salgado, G.F.; Queiroz, J.A.; Cruz, C. Fluorescent Light-up Acridine Orange Derivatives Bind and Stabilize KRAS-22RT G-Quadruplex. *Biochimie* **2018**, *144*, 144–152, doi:10.1016/j.biochi.2017.11.004.

 doi:10.20944/preprints202604.1302.v1

54. Lin, C.; Wu, G.; Wang, K.; Onel, B.; Sakai, S.; Shao, Y.; Yang, D. Molecular Recognition of the Hybrid-2 Human Telomeric G-Quadruplex by Epiberberine: Insights into Conversion of Telomeric G-Quadruplex Structures. *Angewandte Chemie* **2018**, *130*, 11054–11059, doi:10.1002/ange.201804667.
55. Falanga, A.P.; Cremonini, M.; Bartocci, A.; Nolli, M.G.; Terracciano, M.; Volpi, S.; Dumont, E.; Piccialli, G.; Casnati, A.; Sansone, F.; et al. Calixarenes Meet (TG4T)4 G-Quadruplex: Exploring Reciprocal Interactions to Develop Innovative Biotechnological Applications. *Int. J. Biol. Macromol.* **2025**, *305*, doi:10.1016/j.ijbiomac.2025.141331.
56. Guarra, F.; Marzo, T.; Ferraroni, M.; Papi, F.; Bazzicalupi, C.; Gratteri, P.; Pescitelli, G.; Messori, L.; Biver, T.; Gabbiani, C. Interaction of a Gold(I) Dicarbene Anticancer Drug with Human Telomeric DNA G-Quadruplex: Solution and Computationally Aided X-Ray Diffraction Analysis. *Dalton Transactions* **2018**, *47*, 16132–16138, doi:10.1039/C8DT03607A.
57. Canale, T.D.; Sen, D. Hemin-Utilizing G-Quadruplex DNAzymes Are Strongly Active in Organic Co-Solvents. *Biochimica et Biophysica Acta (BBA) - General Subjects* **2017**, *1861*, 1455–1462, doi:10.1016/j.bbagen.2016.11.019.